TISSUE ENGINEERING: Part C
Volume 18, Number 3, 2012

DOI: 10.1089/ten.tec.2011.0343

Nondestructive Evaluation of Tissue Engineered Articular Cartilage Using Time-Resolved Fluorescence Spectroscopy and Ultrasound Backscatter Microscopy

Yang Sun, Ph.D.,[1] Donald Responte, B.S.,[2] Hongtao Xie, Ph.D.,[1] Jing Liu, Ph.D.,[1]
Hussain Fatakdawala, B.S.,[1] Jerry Hu, Ph.D.,[1] Kyriacos A. Athanasiou, Ph.D.,[1] and Laura Marcu, Ph.D.[1]

The goal of this study is to evaluate the ability of a bimodal technique integrating time-resolved fluorescence spectroscopy (TRFS) and ultrasound backscatter microscopy (UBM) for nondestructive detection of changes in the biochemical, structural, and mechanical properties of self-assembled engineered articular cartilage constructs. The cartilage constructs were treated with three chemical agents (collagenase, chondroitinase-ABC, and ribose) to induce changes in biochemical content (collagen and glycosaminoglycan [GAG]) of matured constructs (4 weeks); and to subsequently alter the mechanical properties of the construct. The biochemical changes were evaluated using TRFS. The microstructure and the thickness of the engineered cartilage samples were characterized by UBM. The optical and ultrasound results were validated against those acquired via conventional techniques including collagen and GAG quantification and measurement of construct stiffness. Current results demonstrated that a set of optical parameters (e.g., average fluorescence lifetime and decay constants) showed significant correlation ($p < 0.05$) with biochemical and mechanical data. The high-resolution ultrasound images provided complementary cross-section information of the cartilage samples morphology. Therefore, the technique was capable of nondestructively evaluating the composition of extracellular matrix and the microstructure of engineered tissue, demonstrating great potential as an alternative to traditional destructive assays.

Introduction

Cartilage degeneration is a critical problem in orthopedic medicine and it affects millions worldwide. For example, osteoarthritis affects an estimated 10% of people over the age of 60.[1] The acellularity and avascularity of cartilage contribute to its limited healing capacity, which has created a pressing need for novel tissue regeneration strategies. Toward this end, neocartilage has been formed using a scaffold-free, self-assembling process,[2] during which individual cells are driven by the differential adhesion hypothesis to organize into large tissues.[3] Cartilage constructs produced thus can be modulated by several anabolic[4,5] and catabolic[6,7] exogenous agents to alter their matrix composition and biomechanical properties to attain properties approaching those of native tissue.

The success in developing a useful engineered tissue construct relies heavily on evaluating its structural and biochemical properties both before and after implantation. Traditional destructive methods such as biochemistry assays and mechanical testing are a clear impediment to such a setting and are highly costly and inefficient. Destructive measurements are undesirable in tissue engineering, because cell culturing and differentiation are expensive and time consuming. In addition, conventional methods do not allow nondestructive time-lapse measurements on the same construct that are important for long-term tissue studies. Thus, there is a clear need for nondestructive tissue characterization methodology that allows ongoing evaluation of tissue during development or modification by exogenous agents.

Fluorescence-based techniques have the potential to measure biochemical changes in tissue in relation to clinical diagnosis.[8] Auto-fluorescence of structural proteins (collagen and elastin), co-enzyme factors (the reduced form of nicotinamide adenine dinucleotide, NADH), amino acids (tryptophan, tyrosine), lipids, and vitamins allow label-free compositional analysis of samples.[9] Laser-induced fluorescence has been widely employed in characterizing skin tumors, urinary bladder tumors, head and neck cancer,[10] and myocardial tissue.[11] However, techniques based on the analysis of intensity and spectral distribution of fluorescence are often hampered by challenges in resolving the broad

[1]Department of Biomedical Engineering, University of California Davis, Davis, California.
[2]Department of Bioengineering, Rice University, Houston, Texas.

emission spectra and spectral overlap of the endogenous fluorophores. Time-resolved fluorescence spectroscopy (TRFS) techniques take into account the decay characteristics of the fluorescence emission, thus providing better differentiation between fluorophores with overlapping spectra.[12,13] Additionally, the fluorescence decay characteristics allow description of the biological microenvironment of the fluorophore. This makes TRFS a more robust method for nondestructive tissue analysis. The use of auto-fluorescence in tissue engineering, however, is fairly recent. Previous work includes nondestructive *in situ* evaluation of osteogenic differentiation with TRFS[14] and TRFS and ultrasound evaluation of cartilage constructs cultured in scaffolds.[15] Collagen, glycosaminoglycan (GAG), and NADH are major endogenous fluorophores of engineered tissue that can be analyzed using fluorescence spectroscopy. Formation or degradation of collagen, collagen crosslinks, and changes in relative concentration of other fluorophores will change the overall tissue fluorescence emission.

Ultrasound imaging is well recognized as a viable tool for studying the structure and morphology of biological tissue.[16,17] Moreover, ultrasound backscatter microscopy (UBM) that employs high-frequency transducers (>40 MHz) has been used to characterize atherosclerotic lesions,[18] connective tissue network,[19] and collagen fiber distribution in human dermis.[20] It provides a spatial resolution of tens of microns and sufficient penetration depth of 5–6 mm in soft tissue. For example, a native bovine cartilage sample imaged with 40 MHz ultrasound demonstrated a penetration depth of 4.5 mm.[21] We have previously demonstrated the use of UBM in atherosclerotic plaque characterization studies.[22,23] High-frequency ultrasound was also used to assess the morphologic, acoustic, and mechanical properties of articular cartilage.[21]

The characterization of the tissue engineered cartilage will benefit from the bimodal diagnostic approach combining TRFS and UBM techniques. TRFS provides information on the construct biochemical composition, but this is limited to the thin layers (<0.5 mm) within the ultraviolet (UV) light penetration depth. In addition, no structural information is retrieved. In contrast, tissue evaluation based on UBM enables three-dimensional evaluation of tissue microstructure, morphology and possible structural defects, but lacks information on tissue biochemical content. Thus, TRFS and UBM methods can complement each other, providing better noninvasive characterization and evaluation of the cartilage sample than either modality alone. Moreover, since UBM and TRFS techniques can be easily integrated in fast scanning systems as recently reported,[22,23] such a bimodal approach would enable further development of compact devices for simultaneous evaluation of tissue biochemical composition and structure/morphology.

The overall objective of this study was to evaluate the ability of an experimental system combining TRFS and UBM modalities for nondestructive analysis of changes in the biochemical, structural, and mechanical properties of self-assembled cartilage. Biochemical changes in constructs were induced via exogenous agents able to alter the extracellular matrix (ECM) composition of constructs and subsequently modulate their mechanical properties. In contrast to our previous work employing scaffold-based constructs,[15] in the current study, we investigated self-assembled cartilage constructs. In addition, different strategies to study the ability of TRFS and UBM to detect changes in tissue constructs were used. In this study, all measurements were carried out at one time point of tissue maturation (4 weeks). At this rather advanced maturation time point, tissue biochemical composition was altered chemically in a manner that affected specific components of the ECM (e.g., collagen and GAG). The current approach enabled the induction of controlled changes in the ECM composition in contrast with the earlier study where cells seeded in scaffolds underwent time-lapse differentiation in culture media, the ECM formed over time after a natural course, and the TRFS and UBM measurements were conducted at distinct time points during differentiation. Specifically, the goals of the current study were (1) to determine whether controlled biochemical changes induced in tissue constructs via a set of anabolic or catabolic agents known to affect the collagen or GAG composition can be detected using nondestructive bimodal TRFS-UBM measurements; and (2) to correlate optical and ultrasonic parameters of constructs with biochemical and biomechanical properties of constructs.

Materials and Methods

Tissue fluorophores

To understand the overall fluorescence emission (intensity, emission peak, decay characteristics or lifetime) originating from the engineered cartilage tissue, TRFS measurements were performed in all major intrinsic fluorophores within the sample. These included collagen type II (major collagen type in week 4 engineered cartilage), GAG (providing compressive resistance to the tissue), aggrecan (backbone of the protein-sugar complex proteoglycan), and NADH (expressed in the cells). These measurements served as references. The measurements were conducted in pure powder form for collagen, GAG (chondroitin sulfate), and aggrecan and in 1 mM phosphate-buffered saline solution for NADH. All the chemicals were extracted from tissues or cells and purchased from Sigma-Aldrich.

Cartilage sample preparation and treatments

Bimodal TRFS and UBM measurements were performed on self-assembled articular cartilage samples generated as follows. Chondrocytes were harvested from the patellofemoral groove and distal femur of immature bovine (Research 87) as described previously.[7] Cells were seeded at a high density (5.5 million cells in 100 μL) in 5 mm diameter agarose wells to form constructs cultured at 37°C, 10% CO_2 and were fed daily with a chemically defined, chondrogenic medium.[7] The cells aggregated and formed constructs via cell-cell interactions and later produced matrix to increase integrity; mechanical data verify that self-assembly created robust constructs. Details concerning construct formation and maturation have been addressed in our previous work.[3] All exogenous agents were administered in chondrogenic medium, and constructs were cultured at 37°C, 10% CO_2 for the duration of each respective treatment. For the collagenase treatment, constructs were exposed to 0.2% collagenase for 30 min. Chondroitinase-ABC (C-ABC) treated constructs were each incubated in 500 μL of a 2 U/mL C-ABC solution for 4 h. Ribose treatment was performed for 4 h at a

concentration of 30 mM. Collagenase is responsible for the degradation of the collagen components, while C-ABC depletes GAG content. Ribose can nonspecifically oxidize the collagen to form crosslinks. These treatments targeted in modifying the collagen and GAG contents in the cartilage construct. At 4 weeks, the constructs were assessed using nondestructive assessments and then processed for biochemical and biomechanical testing. The different treatments were applied at the end of tissue culture (i.e., directly before optical and mechanical testing). This enabled us to optimize the different matrix compositions to observe any differences in optical or conventional assessments. Based on histology of control samples and previous work,[2,3] we estimated the biochemical composition as being relatively uniform throughout the construct. The treatment applied to constructs also exhibited relatively uniform depletion of GAGs and collagen for C-ABC and collagenase treatments, respectively. Consequently, the central 3 mm regions of the constructs were used for compressive evaluation, and the outer ring was used for biochemical assays and tensile evaluation.

TRFS-UBM system and measurements

The hybrid TRFS-UBM system consists of four primary modules: TRFS sub-system, UBM sub-system, hybrid probe, and control unit (Fig. 1).

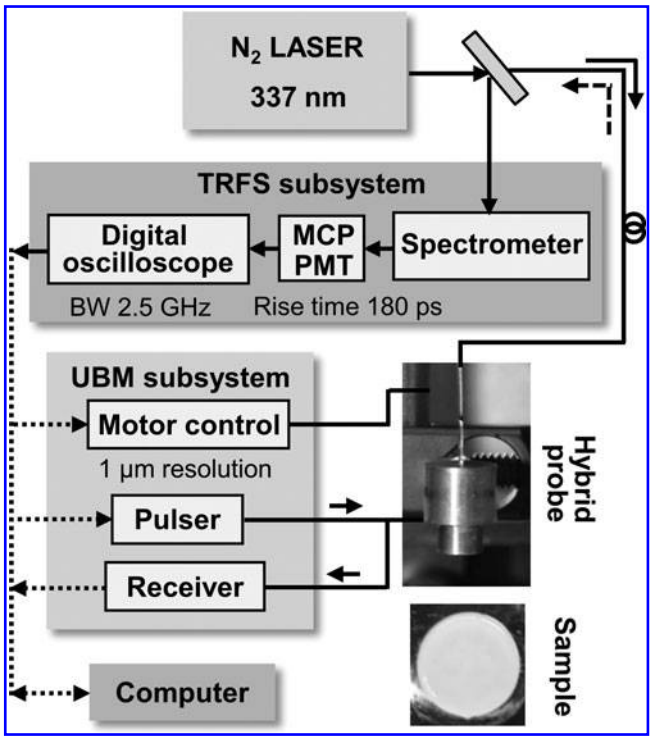

FIG. 1. A schematic diagram of the combined TRFS-UBM system including laser source module, TRFS subsystem, UBM subsystem, and the combined probe (transducer and fiberoptic). A tissue engineered cartilage sample (at t = week 4) is shown. TRFS, time-resolved fluorescence spectroscopy; UBM, ultrasound backscatter microscopy; MCP, multichannel plate; PMT, photomultiplier tube.

TRFS sub-system. A pulsed nitrogen laser (337 nm, 0.7 ns, 30 Hz) provided the excitation light through an optical fiber (600 μm core diameter, numerical aperture = 0.22), which was positioned perpendicular to the sample and directed light onto the sample. Sample autofluorescence was collected through the same fiber and a beam splitter, and dispersed by a spectrophotometer after which scattered excitation light was removed by the use of a long-pass filter (340 nm). The fluorescence signal was detected with a gated multichannel plate photomultiplier tube (rise time of 180 ps), and amplified by a wideband preamplifier (1.5 GHz bandwidth), recorded by a fast digitizer (2.5 GHz bandwidth, 20 G samples/s). The fluorescence decay pulses from each sample were obtained by scanning of the spectrophotometer across a spectral range of 360–600 nm (steps of 5 nm). The laser output energy was measured at the end of the optical fiber and was adjusted to 2 μJ/pulse providing a fluence of 0.7 mJ/cm^2, which was far below the ANSI limit for Maximum Permissible Exposure of UV light excitation (3 mJ/cm^2). Measurements were taken from four locations on each sample, with the probe placed in direct contact with the sample. Reflected laser pulses from the sample were measured after the fluorescence measurements for the deconvolution of the system response from the measurements.

UBM subsystem. A high-voltage pulser generating a wideband pulse (200 V peak-to-peak) was used to drive the ultrasound transducer. The received radiofrequency (RF) echoes were amplified with a 30 dB low-noise amplifier and filtered with a bandpass filter (24–90 MHz). A 12-bit digitizer with a sampling rate of 400 M samples/s was employed to record the RF. A linear positioning stage (1 μm positioning resolution) allowed for scanning and forming a UBM image. The measurements were conducted with a customized 40 MHz press-focused single element transducer (aperture size of 3.75 mm, 63% bandwidth, 6 mm focal depth) made available by the Ultrasonic Transducer Resource Center, University of Southern California, Los Angeles, CA. The optical fiber for TRFS measurements was inserted in the center channel (0.9 mm diameter) of the transducer. The UBM system with this transducer provided an axial and lateral resolution of 30 and 65 μm, respectively.

Biochemical, histological, and mechanical testing

For biochemical analysis, samples were frozen at −20°C and lyophilized for 48 h to determine dry weights. Lyophilized samples were digested using pepsin-elastase as previously described.[11] DNA content was determined using PicoGreen® dsDNA Assay Kit (Invitrogen). Sulfated GAG content was assayed using the Blyscan Glycosaminoglycan Assay kit (Biocolor), and collagen content was quantified using a chloramine-T hydroxyproline assay.[24] For histology, samples were cryo-embedded and then sectioned at 14 μm. Sections were fixed in formalin and stained with safranin-O/fast green and picrosirius red.

Compressive properties were quantified using a creep indentation apparatus.[25,26] A 0.8 mm, a porous indentation tip was used to apply a tare load of 0.2 g followed by a test load of 0.7 g. For tensile testing, samples were cut into dog-bone shapes and glued to paper tabs for testing.

Tensile assessments were conducted at a strain rate of 1% of the gauge length per second on a materials-testing system (Instron Model 5565). The slope of the resulting stress-strain curve yielded the Young's modulus, and the maximum stress was reported as the ultimate tensile strength.

Fluorescence and ultrasonic data processing

Fluorescence system response was fully characterized by the shape of its fluorescence decay profile, $h(k)$ for $k=0\ldots K-1$, where k was the index for the $(k+1)$th time sampling point with a sampling rate of 20 G samples/s ($\delta_t=0.05$ ns). The fluorescence decay function $h(k)$ was assumed to follow a bi-exponential (BE) decay model,[27] where $h(k)$ was a weighted average of two exponential decay functions with two time constants, τ_1 and τ_2 [Equation (1)]:

$$h(k)=\sum_{j=1}^{2}\alpha_i e^{-\frac{(\delta t)\cdot k}{\tau_i}}, for\ k=0\ldots K-1 \quad (1)$$

α_1 and α_2 were the amplitude of the components at $t=0$, and τ_1 and τ_2 were estimated from time-resolved fluorescence responses. However, we should emphasize that, with BE model, we did not implicitly assume that the fluorescence system under study was composed of two distinct fluorescent species. Rather, the choice of the number of exponential decay components was merely justified by the goodness of fit. The time constants for the two components were considered as averaged time scales for fast components and slow components in the fluorescence system, respectively.

The average lifetime can be calculated as Equation (2),

$$\tau_{avg}=\frac{\delta t\cdot\sum_k kh(k)}{\sum_k h(k)} \quad (2)$$

Incidentally, for the BE model with decay profile in (1), Equation (3) gives,

$$\tau_{avg}^{BE}=\frac{\alpha_1\tau_1^2+\alpha_2\tau_2^2}{\alpha_1\tau_1+\alpha_2\tau_2} \quad (3)$$

The fractional contribution for each time constant to the average lifetime was defined as Equation (4):

$$A_1=\frac{\alpha_1\tau_1}{\alpha_1\tau_1+\alpha_2\tau_2}, A_2=\frac{\alpha_2\tau_2}{\alpha_1\tau_1+\alpha_2\tau_2} \quad (4)$$

The fluorescence spectrum was obtained by integration of the measured fluorescence decay curves over time. The fluorescence spectra were normalized by maximum fluorescence intensity along the entire emission wavelength.

The ultrasound image was formed by subtracting the DC offset from the ultrasonic RF data, and a band-pass filter with a frequency range of 24 to 75 MHz was used to remove high-frequency noise. The Hilbert transform was applied to the filtered RF signals to detect the envelopes, followed by a logarithmical compression. The processed data for each line of sight were displayed to form a gray-scale B-mode ultrasound image showing the reconstruction of the cross section of the tissue constructs.

Statistical and correlation analysis

Six samples were assessed with conventional biochemical and biomechanical tests, as well as nondestructive optical and ultrasonic measurements for each group (total of 24 samples). Four nonoverlapped locations were randomly chosen from each sample for repeated fluorescence measurements. The parameters reported for each sample represent the average of the parameter values retrieved from the four measurements. A one-way ANOVA test was used to analyze the data, and Tukey's *post hoc* test was used when warranted. Significance was defined as $p<0.05$. All the data were presented as mean ± standard deviation. Pairwise comparisons were generated between all optical and conventional parameters, and correlation coefficients with $p<0.05$ were considered significant. Correlation coefficients are reported in the results.

Results

TRFS of tissue fluorophores

The fluorescence emission characteristics obtained from the major intrinsic fluorophores in cartilage tissue are presented in Figure 2. Collagen showed significantly stronger fluorescence intensity than all other fluorescent components (Fig. 2a). While the fluorescence spectral shape of GAG (chondroitin sulfate) strongly overlapped (emission peak at ~400 nm) that of collagen (Fig. 2b), the intensity of GAG was significantly lower by 6.5 times. Both aggrecan and NADH had red-shifted emission peaks at ~450 and ~465 nm, respectively (Fig. 2b). Collagen exhibited the longest lasting emission among all fluorophores as demonstrated by both the average lifetime value (~5.6 ns at 400 nm; Fig. 2c) and the slow decay time component τ_2 value (~6.7 ns at 400 nm; Fig. 2d) that accounted for ~80% of the overall decay (Fig. 2e). GAG also presented a relatively long-lasting emission with an average lifetime slightly lower than collagen (~4.3 ns at 400 nm) and slightly different decay dynamics characteristics (~5.0 ns τ_2 and ~83% A_2). Aggrecan presented faster decay dynamics (~3.1 ns $\tau_{average}$, ~4.4 ns τ_2, and ~65% A_2 at 400 nm) when compared with both collagen and GAG. The NADH in free form presented very fast decay dynamics with an average lifetime in sub-nanosecond range (~0.38 ns at 465 nm) as previously reported.[9]

TRFS of cartilage constructs

The time-resolved fluorescence spectra of the four groups (control, collagenase, C-ABC, and ribose) were described by various combinations of spectroscopic parameters as a function of wavelength (Fig. 3). The cartilage samples treated with collagenase had degraded collagen content and presented a significantly lower intensity (by 33%) compared with the control group which showed the highest intensity in the 400–460 nm spectral range (Fig. 3a). The emission spectra of all groups were largely overlapped (peak at ~430 nm), except for the control group that showed a slightly blue-shifted peak emission (~415 nm; Fig. 3b). Major changes of the average lifetimes of all the groups occurred at the wavelength band of 400/40 nm instead of the fluorescence emission peak of 430 nm. The average lifetimes were elevated at 400/40 nm and then decreased when the

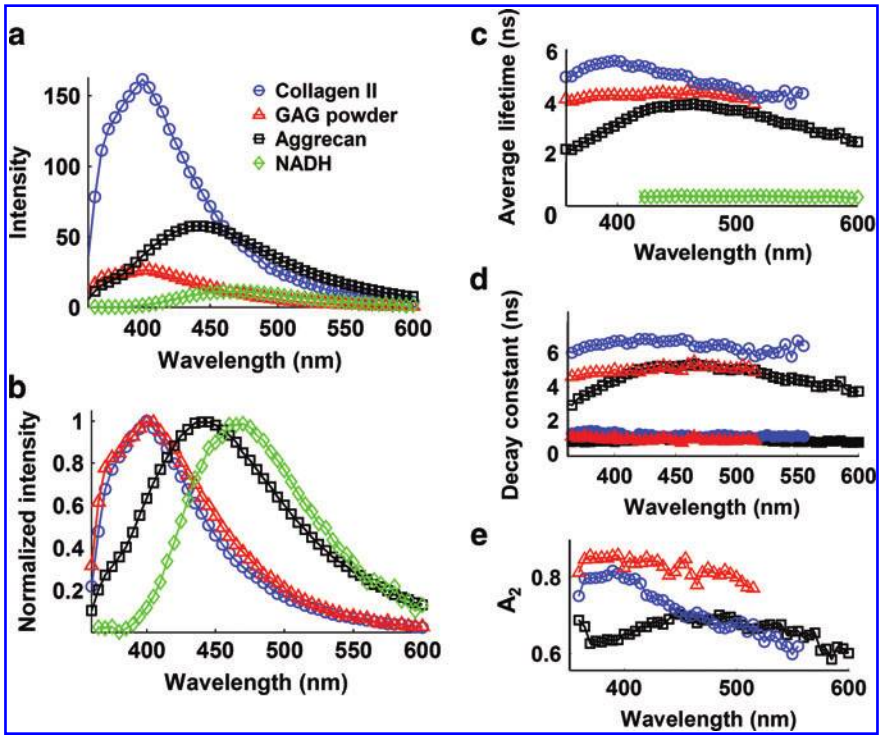

FIG. 2. Fluorescence spectroscopic data acquired from the major endogenous fluorophores in the cartilage samples, including collagen type II, GAG powder, aggrecan, and NADH in cells. The time-resolved fluorescence parameters were retrieved with bi-exponential deconvolution. **(a)** Plots of fluorescence spectrum, **(b)** normalized spectrum, **(c)** average lifetime, **(d)** fast decay constant τ_1 (filled symbols) and slow decay constant τ_2 (open symbols) for collagen, GAG, and aggrecan (since NADH has only one exponential component, NADH was not included here), and **(e)** the fractional contribution of the slow decay component A_2. GAG, glycosaminoglycans; NADH, the reduced form of nicotinamide adenine dinucleotide. Color images available online at www.liebertonline.com/tec

wavelength increased (Fig. 3c). The control and C-ABC groups, which contained higher collagen concentration than the collagenase treated group (C-ABC selectively digested GAG and allowed it to leach out, therefore increasing collagen concentration), exhibited longer-lasting emission compared with other groups as demonstrated by the average lifetime value of ~2.8 ns (Fig. 3c) and the dynamics characteristics (τ_2 of ~3.8 ns and A_2 of ~70%; Fig. 3d, e). The samples of the collagenase group with degraded collagen showed fast decay dynamics ($\tau_{average}$ of ~2.4 ns at 400/40 nm, τ_2 of ~3.4 ns, and A_2 of ~65%). There was no significant difference for the fast decay components τ_1 for all the

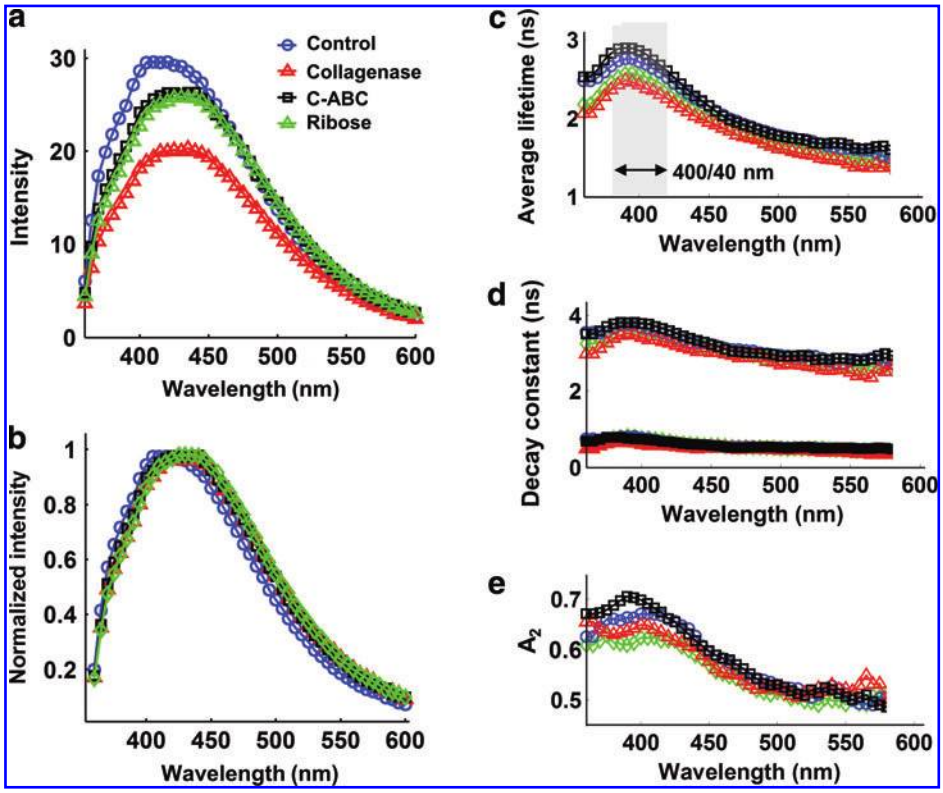

FIG. 3. Fluorescence spectroscopic data acquired from four groups of cartilage samples with different treatments (control, collagenase, C-ABC, and ribose). The time-resolved fluorescence parameters were retrieved with bi-exponential deconvolution. **(a)** Fluorescence emission spectrum, **(b)** normalized spectrum, **(c)** average lifetime, **(d)** fast decay constant τ_1 (filled symbols) and slow decay constant τ_2 (open symbols), and **(e)** fractional contribution of the slow decay component A_2. C-ABC, chondroitinase-ABC. Color images available online at www.liebertonline.com/tec

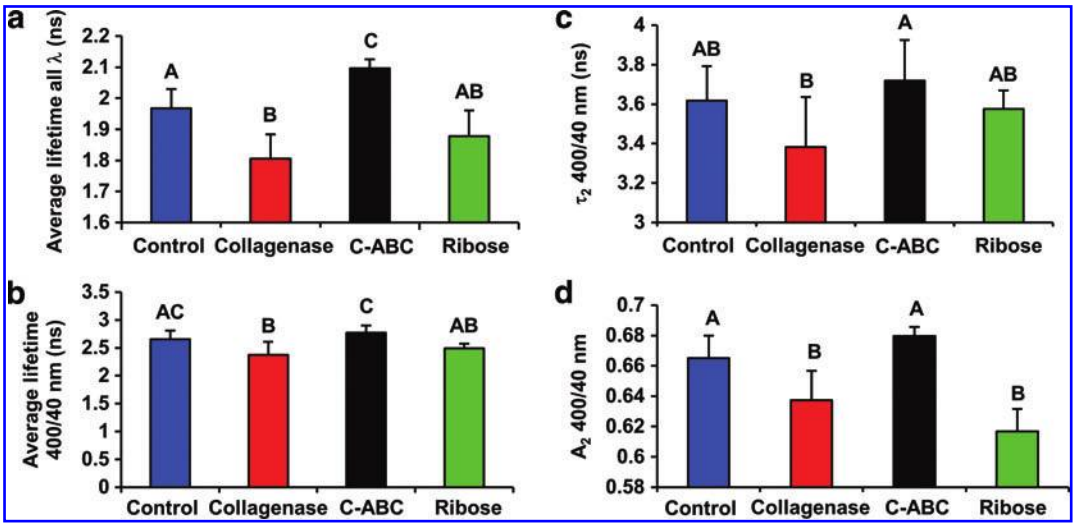

FIG. 4. Quantification of the time-resolved fluorescence parameters for the four groups. **(a)** The mean value of the average lifetime from 360 to 600 nm, **(b)** average lifetime at 400/40 nm, **(c)** slow decay constant τ_2 at 400/40 nm, and **(d)** fractional contribution of the slow decay component A_2. The letters above the bars were used to show the groups with significant difference. For example, in **(a)**, the average lifetime over all wavelength of the control group (labeled as A) was significantly different than the average lifetime of the collagenase group (labeled as B; $p < 0.05$). There was no significant difference for groups labeled with same letters. Such as in **(a)**, no significant difference was observed for the average lifetime between the control group (labeled as A) and the ribose group (labeled as AB). Color images available online at www.liebertonline.com/tec

groups obtained from bi-exponential deconvolution (0.7 ns at 400 nm; Fig. 3d). The fractional contribution of the slow decay A_2 had a greater effect on the average lifetime than A_1 and showed more differences among groups (Fig. 3e).

A set of time-resolved parameters were statistically analyzed for each treatment group and summarized in Figure 4. Some differences in optical parameters between the groups were observed through the entire emission wavelength range; thus, we evaluated the overall changes in parameters values in order to achieve better differentiation between treatments. Thus, the mean value of average lifetimes was calculated over the whole wavelength range from 360–600 nm, then the lifetime value of the C-ABC group was significantly longer than that of the control group (Fig. 4a). In addition, since specific wavelength band can be used in order to understand the changes related to a specific fluorophore (i.e., collagen), the average lifetime at 400/40 nm was evaluated. It was found that the lifetime of the collagenase group was significantly lower than those of the control and C-ABC groups (Fig. 4b), though no significant difference was shown between the C-ABC and control groups. Information from red-shifted wavelength helped with differentiation between C-ABC and control groups as depicted in Figure 4a and b. For the slow decay constant τ_2 at the wavelength band of 400/40 nm, the τ_2 value of the constructs treated by C-ABC was significantly increased by 12% than the τ_2 of the collagenase group, indicating that this parameter related to the increase of the collagen concentration (Fig. 4c). The slow decay constant τ_2 contributed to >60% of the overall fluorescence emission regardless of treatment (Fig. 4d). The fractional contribution of the slow decay constant A_2 of the collagenase group was also significantly lower than those of the control and C-ABC groups (Fig. 4d). The combination of τ_2 and A_2 resulted in a significant faster decay and shorter average lifetime for the collagenase group compared with the control and C-ABC groups.

UBM images of cartilage constructs

UBM images of the cross section of the cartilage samples from the four treatment groups are shown in Figure 5. The thickness of each sample could be determined at multiple points by measuring the distances from the top and bottom surfaces of the UBM images, and an average thickness (taken from 10 different locations) was used to compare thickness among the groups (Fig. 5b). The collagenase group was found to have a significantly lower thickness of 0.22 ± 0.02 mm compared with a thickness of 0.41 ± 0.04 mm for the control group, a decrease of 46%. By observing the morphological features of the cartilage constructs from the UBM images, the surfaces of the samples were well defined with a relatively uniform region within the margins (Fig. 5a). In addition, a hyperechoic region was shown in the area of the edges for some of the cartilage constructs compared with the center of the sample (Fig. 5a). For example, the average intensity of backscatter signals at the left edge of the sample in C-ABC group was ~6 dB greater than the echo intensity from the center of the sample.

Histology

Histology results are summarized in Figure 6. Picrosirius red staining showed decreased collagen abundance in collagenase-treated samples, whereas the other two treatment groups exhibited similar staining intensities as the control (Fig. 6a). Safranin-O/fast green stained the control and ribose groups more heavily for GAG (red staining) than the collagenase or C-ABC treatment groups (Fig. 6b). A secondary effect of collagenase digestion was GAG depletion, which

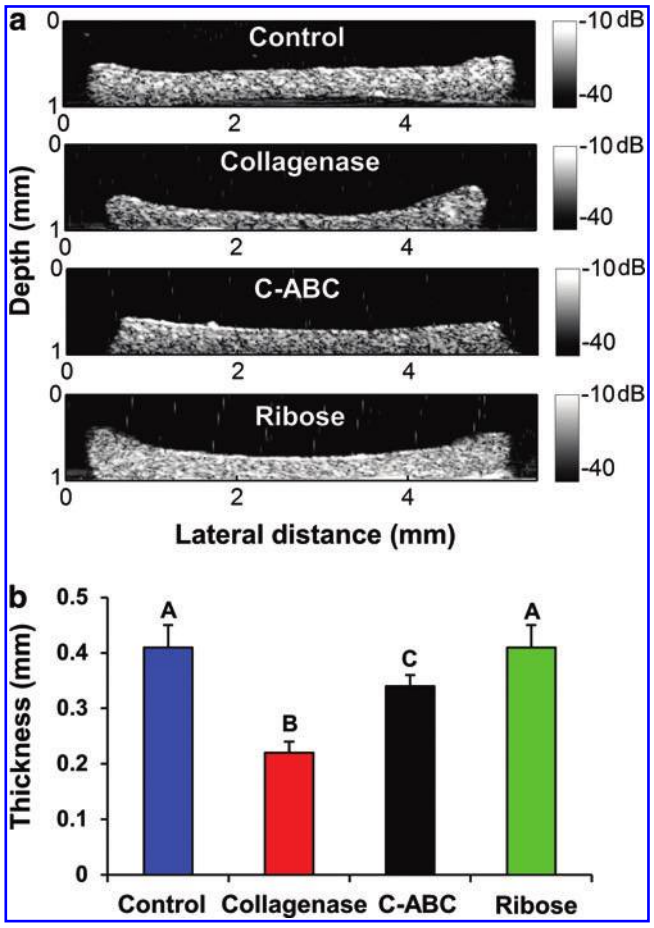

FIG. 5. **(a)** UBM images of the cartilage samples from the four groups. The shading values were intensity values displayed in dB scale. **(b)** Thickness measurements of samples for each group. The letters above the bars were used to show the groups with significant difference. Color images available online at www.liebertonline.com/tec

occurred due to the lack of an intact collagen network to entrap GAG complexes. C-ABC administration resulted in less GAG staining than the collagenase treatment.

Biochemical and biomechanical results

Biochemical and biomechanical assessments are shown in Figure 7. Collagen content decreased significantly after collagenase treatment and increased significantly with C-ABC treatment (Fig. 7a). Ribose treatment did not statistically alter collagen content. GAG content decreased for constructs treated with either collagenase and C-ABC, resulting in GAG/WW values of 5.1% and 3.1% for collagenase and C-ABC treatments, respectively (Fig. 7b). The Young's modulus value, E_Y, significantly decreased after collagenase treatment. In contrast, tensile strength increased after both C-ABC and ribose treatments by 72% and 49%, respectively (Fig. 7c). Compressive stiffness decreased significantly for both collagenase and C-ABC treatment groups. Aggregate modulus values were 70 and 36 kPa for the collagenase and C-ABC treatment groups, respectively. Ribose treatment did not significantly alter the compressive stiffness (Fig. 7d).

Correlation with optical, biochemistry, and biomechanical properties

The correlation test was performed for all optical parameters (lifetime, decay constants, and intensity). One of these parameters with the highest correlation coefficient (average lifetime over 400/40 nm) is shown in Figure 8. Parameters between the nondestructive and destructive assays (optical, biochemistry, and biomechanical methods) with high and significant correlation are presented here. The time-resolved parameters such as τ_{390}, τ_{450}, τ_{1-390}, and τ_{1-450} showed high correlation ($r > 0.45$) and significant correlation with both collagen/ww and E_Y. Significant and high correlation was observed for collagen/ww with E_Y ($r = 0.81$) and for collagen/ww with average lifetime over the wavelength band of 400/40 nm ($r = 0.69$; Fig. 8a). Significant and high correlation was also observed for GAG/ww with H_A ($r = 0.70$). However, no significance was found between GAG/ww and the average lifetime over 400/40 nm ($r = -0.26$; Fig. 8b). Notably, significant and high correlation was observed between the average lifetime over 400/40 nm and E_Y ($r = 0.57$), but no significance was found between the average lifetime and H_A ($r = -0.07$; Fig. 8c).

Discussion

Biochemical compositions and TRFS results

Given the biochemical content of cartilage tissue constructs, the most likely auto-fluorescent biomolecules in these constructs are the constituents of the ECM (collagen type II, crosslinks, GAGs, and aggrecan) and the NADH in cells. The fluorescence emission of these biological fluorophores was studied (Fig. 2), and the emission characteristics of collagen

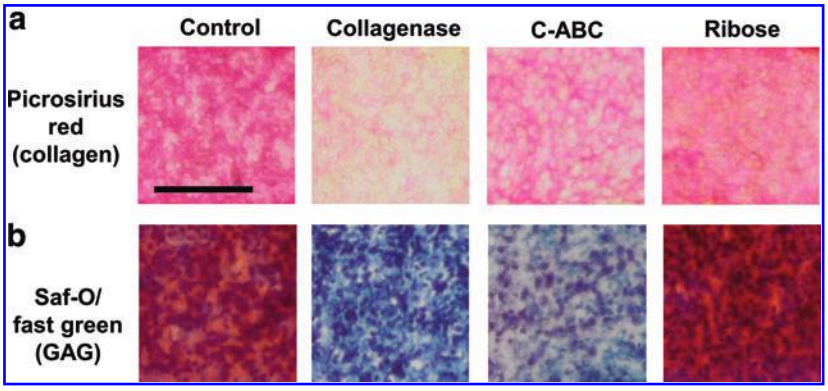

FIG. 6. Histology results with **(a)** picrosirius red for collagen and **(b)** safranin-O/fast green for GAG. The scale bar corresponds to 100 μm. Color images available online at www.liebertonline.com/tec

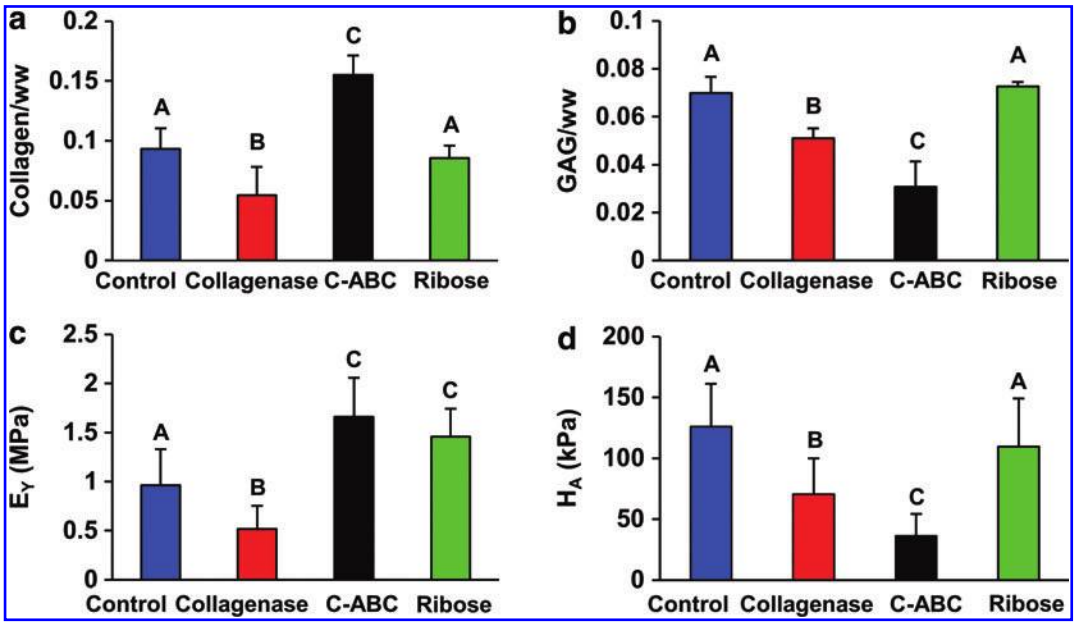

FIG. 7. Biochemistry results for the quantification of **(a)** collagen content and **(b)** GAG content normalized by wet weight of the sample. Biomechanical results for **(c)** Young's modulus and **(d)** aggregate modulus for the four groups. The letters above the bars were used to show the groups with significant difference. Color images available online at www.liebertonline.com/tec

and NADH were found to be consistent with values in literature.[9,28] While GAG demonstrated a peak fluorescence emission at about 400 nm, similar to the emission peak of collagen, GAG emission measured in tissue extracts for the same excitation fluence rate was found to be more than six times weaker than that of collagen (Fig. 2a). This suggested that (1) GAG had less contribution to the overall fluorescence emission due to the weak emission intensity and (2) the collagen emission characteristics were most likely to dominate the whole emission when both collagen and GAG molecules were present. The fluorescence spectrum of aggrecan alone showed an emission peak of 450 nm, close to the emission peak of the spectrum of the cartilage sample (420–430 nm), demonstrating the contribution of aggrecan to the cartilage autofluorescence (Fig. 2a). To the best of our knowledge, this is the first time that time-resolved fluorescence spectroscopic data for GAG and aggrecan have been reported.

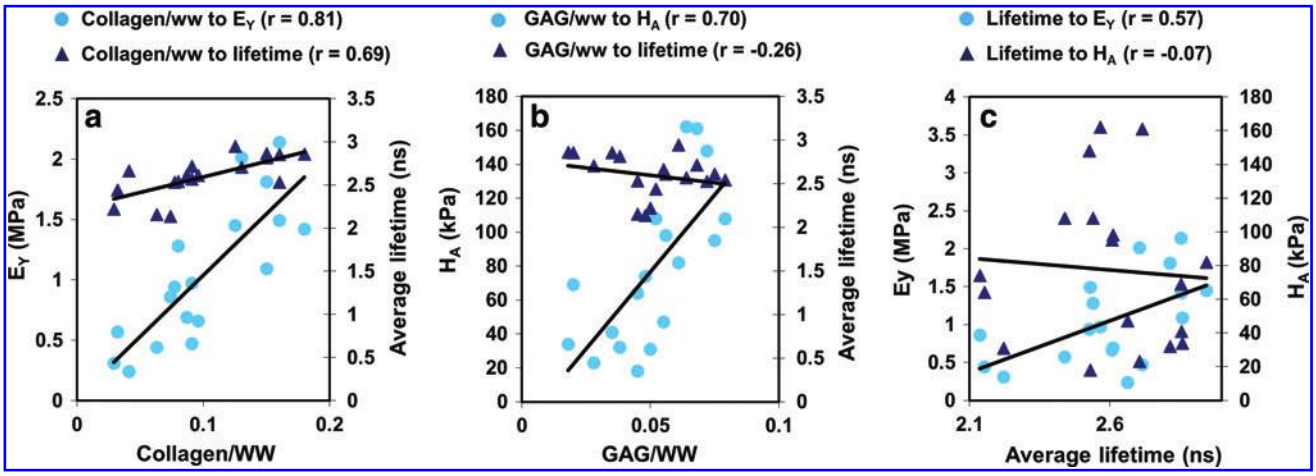

FIG. 8. **(a)** Correlations between collagen/ww and E_Y (Pearson $r=0.81$, $p<0.0001$) and between collagen/ww and mean value of the average lifetime over the wavelength range of 400/40 nm (Pearson $r=0.69$, $p=0.0015$). **(b)** Correlations between GAG/ww and H_A (Pearson $r=0.70$, $p=0.0012$) and between GAG/ww and the average lifetime over 400/40 nm (Pearson $r=-0.26$, $p=0.31$). **(c)** Correlations between the average lifetime over 400/40 nm and E_Y (Pearson $r=0.57$, $p=0.01$) and between the average lifetime over 400/40 nm and H_A (Pearson $r=-0.07$, $p=0.77$). Data of the ribose group were taken out from the correlation test, as ribose did not change the compositions in the cartilage constructs. Color images available online at www.liebertonline.com/tec

The TRFS results obtained for cartilage constructs showed varied blue-shifted fluorescence intensity and average lifetime values at 400 nm among the treatments, suggestive of contribution by mature collagen. Collagen typically presents a peak emission at 390–400 nm and has a lifetime of >5 ns, longer than the lifetime of other fluorophores in the construct. The statistically significant decreases in average fluorescence lifetime values at 400/40 nm ranging from 2.65 ns in control samples to 2.37 ns in collagen-depleted samples (Fig. 4b) were further underscored by the high correlation of collagen/ww with the average lifetime ($r=0.7$, $p=0.0001$) as seen in Figure 8. However, the correlation between GAG/ww and average lifetime was not significant ($p=0.09$), suggesting that collagen dominated the fluorescence emission and that, most likely, GAG has a smaller contribution to the overall cartilage sample emission. These results are consistent with the pure fluorophore analysis in Figure 2. The emission peak of the spectrum of the cartilage constructs was found at ~430 nm (not 400 nm where most of the changes in fluorescence decay characteristics occur), possibly due to the contribution of aggrecan and NADH that exhibit red-shifted fluorescence emission.

Combination of multiple time-resolved fluorescence parameters

Current results suggested that changes in sample collagen concentration (collagen/ww) can be monitored using the fluorescence decay parameters (lifetime averaged over all the emission wavelenghts). For example (Fig. 4a), reduced collagen concentration due to collagenase treatment corresponded to a significant decrease in fluorescence lifetime, while increased collagen concentration due to depleation of GAG induced by C-ABC treatment corresponded to a significant increase in average lifetime values when compared with the control group. These results were confirmed by the biochemical analysis of the samples (Fig. 7a). Analysis of the average lifetime at 400/40 nm wavelength band (coresponding to the largest variability in decay parameters) as a function of treatment type followed similar trends as the analysis for all wavelengths (Fig. 4b). However, a statistical difference was only observed between control and collagenase groups and not for the C-ABC group. As just noted, collagenase was expected to directly affect the collagen content in the sample in contrast to the C-ABC treatment that depleated GAG and indirectly modified the collagen concentration. This suggested that GAG might have had a minor contribution to the overall fluorescence emission of the construct. This assumption was in agreement with the correlation analysis (Fig. 8) that demonstrated the increase in the average lifetime was correlated with increased collagen/ww but not with increased GAG/ww.

Most of the changes of the other fluorescence decay parameters (e.g., τ_2 and A_2) took place at ~400 nm (Fig. 3). This, taken together with the fact that collagen showed (1) an emission peak of 400 nm, (2) a larger τ_2 value compared with other cellular and extracellular components in the sample, (3) an A_2 value greater than 80% at short wavelengths (~400 nm; Fig. 2), and (4) the same trend of A_2 compared with that of the cartilage sample (Figs. 2e and 3e), it was confirmed once again that collagen dominated the fluorescence emission of the constructs. Across the different treatments the statistical analysis of τ_2 and A_2 showed similar trends as that of the average lifetime, as just discussed (Fig. 4c, d). Significant changes were observed between the collagenase and C-ABC groups, between which the greatest difference of the collagen concentration existed. Ribose nonspecifically oxidized the collagen crosslinks and did not directly change the matrix biochemical composition. Thus, no significant or consistent changes in the decay parameters were observed when the ribose group was compared with others (Fig. 4).

In summary, multiple time-resolved parameters retrieved from TRFS data including (1) the fast and slow decay constants τ_1, τ_2, (2) the corresponding fractional contribution A_1, A_2, and (3) the average lifetime at specific wavelength bands allowed for a full characterization of the fluorescence decay dynamics that originated from engineered tissues. The combination of a set of these parameters with the best differentiation capability (parameters showing the most significant difference between treatments) provided a robust and sensitive detection of biochemical compositions of the tissue engineered cartilage samples. Since only the collagen and GAG contents were modified by the chemical treatments and the fluorescence emission of GAG was found much weaker than that of collagen, most likely the changes in TRFS features reported here were generated primarily by changes in collagen content and collagen cross-links. However, TRFS can be used for detection of other endogenous fluorophores besides collagen in cartilage tissue, such as aggrecan or NADH in cells. By using the fluorescence decay characteristics (τ_1, τ_2, and A_2), the relation between the relative concentration of specific component in a mixture of fluorophores and the overall fluorescent signals can be evaluated and quantified. The current results demonstrated that the fast decay constant τ_1 was similar for each group, while the slow decay constant τ_2 and fractional contribution A_2 indicated major changes. For example, collagenase depleted collagen resulting in the decrease of collagen/ww in the sample. From the fluorescence decay signals of the collagenase group, both τ_2 and A_2 decreased compared with other groups, such that the combined effect of these variations caused an overall decrease of average lifetime. Since the major changes in fluorescence signals were from collagen content, the τ_2 was related to the collagen content in the sample, and the decrease of A_2 was related to the decrease of collagen concentration. In this way, the relative concentration of collagen content can be quantitatively resolved. However, this would require additional biochemical tests for the validation of the spectroscopic findings.

Tissue characterization with UBM data

We determined that UBM measurements successfully complemented the optical methods by providing morphological and structural information of the samples' cross section. The UBM system could also measure the thickness of the sample and monitor the samples' changes in shape or profile. The thickness measurement based on the UBM images was more robust than measurements using a caliper due to (1) a natural curvature of the sample that is sometimes present (Fig. 5a) and (2) UBM measurement does not deform the sample during measurement, providing a more accurate assessment. The thickness changes were consistent with the

effects expected of each treatment, as reported in previous studies. For example, the samples treated with collagenase showed a significant decrease of the thickness compared with all other groups because of (1) the removal of collagen from the sample surface and (2) the resultant decrease in GAG content (Fig. 5b) that used to maintain tissue swelling. UBM has the potential to provide a multidimensional analysis of the construct including microstructure, morphology, shape, thickness of the construct, detection of potential defects in the constructs, and, ultimately, the UBM backscatter signals can be used to evaluate the construct mechanical properties.[21] In addition, UBM can differentiate tissue morphological heterogeneity spatially with high resolution ($\sim 50\,\mu m$). As depicted in Figure 5, variation of the echogenicity detected by UBM was related to the changes of tissue density and resulting changes of acoustic impedance, while these local changes in cartilage constructs were not detected significantly by the biochemistry test or TRFS measurements. Compared with other imaging modalities, UBM shows advantages, as it is a noninvasive approach, can reach a penetration depth of 5–6 mm, which is more than 10 times deeper than what is attainable by the optical techniques applied here ($< 250\,\mu m$), and provides competitive high resolution (approximately tens of microns). Optical coherence tomography was used to quantify optical surface reflection and surface roughness of articular cartilage,[29] providing high resolution images ($\sim 10\,\mu m$) but limited penetration depth (~ 1 mm). While modalities for osteoarthritis diagnosis including X-ray,[30] arthroscopy,[31] and magnetic resonance imaging (MRI)[32] have been tested in clinical studies, these techniques have specific limitations. For example, X-ray and arthroscopy are radioactive or invasive approaches, and MRI is limited by resolution and cost. Therefore, the use of UBM in this study has shown great potential for it to be a noninvasive technique to evaluate the structure of cartilage.

Feasibility of noninvasive evaluation with the combined TRFS/UBM

The combined tissue characterization technique, TRFS and UBM, successfully detected collagen changes in tissue construct composition and was found to be strongly correlated with standard biochemical and mechanical analysis. The tissue samples with collagenase treatment showed significantly shorter lifetime at 400/40 nm compared with other groups, as the collagen content was eroded by collagenase (Fig. 4b). C-ABC treatment depleted GAG and, therefore, increased the concentration of collagen, resulting in an increase of average lifetime (Fig. 4a). The collagenase group gave the weakest fluorescence intensity and also the shortest average lifetime, because the collagenase not only degraded the collagen network but also decreased the GAG content. UBM provided parallel information in terms of the growth of the constructs with different types of treatments. The reduced thickness of the collagenase group samples was attributed to the reduction of both the collagen and GAG content, while that of the C-ABC group samples was due to the reduction of GAG content only (Fig. 5). These observations were validated by biochemical results where the collagen/ww of the collagenase group was lowest among the groups and the GAG/ww was lowest for the C-ABC group (Fig. 7). A strong correlation between the average lifetime and collagen/ww was observed, as the fluorescence signals were directly related to the collagen content and crosslinks. Collagen and its crosslinks are directly related with biomechanical properties of the cartilage samples.[33] However, fluorescence parameters were indirectly related to the mechanical properties. Therefore, it showed stronger correlation between optical parameters with biochemical compared to biomechanical properties. In summary, a set of optical parameters (such as average lifetime at specific wavelength bands, decay constants, and fractional contribution) could be used to infer the biochemical and biomechanical properties of engineered tissues.

Conclusion

This article presented techniques for the evaluation of engineered articular cartilage, specifically a combined optical and ultrasound system. This novel TRFS-UBM approach enables assessment of not only the cartilage construct's ECM biochemical composition (changes in collagen content in particular) but also the morphology of the construct, suggesting great potentials of nondestructive testing of engineered cartilage and, thus, has implications for future clinical applications. Significant and high correlations were found between cartilage construct mechanical characteristics and biochemical compositions, such as the correlation between Young's modulus and collagen/ww, as well as aggregate modulus and GAG/ww.[2] These results confirmed previous observations that collagen content contributed to the tensile property of the cartilage and GAG content contributed to the compressive property. The major finding of this study was that significant and high correlation was observed between optical parameters and collagen/ww, but not GAG/ww, suggesting that collagen dominated the overall fluorescence emission of the cartilage sample, and the fluorescence decay parameters could be used as an indicator of changes in collagen content within the cartilage sample. Significant and high correlation was also observed between optical parameters and Young's modulus, suggesting the potential nondestructive assessment of mechanical properties of cartilage samples. The UBM images provided complementary structural reconstruction of the cross section and thickness evaluation of the construct. In addition, they compensated for the penetration depth limitation of the optical technique. The bimodal results demonstrated the feasibility of simultaneous acquisition of fluorescence and ultrasonic data for synergic evaluation of cartilage constructs with such a compact system. Although the function of UBM was limited in this study to the visualization of the structure, measurement of the thickness, and detection of the variation of the cartilage density, UBM could play an important role in future studies for full characterization of microstructure of the cartilage constructs and evaluation of mechanical properties through the analysis of ultrasound RF signals. Current findings are conducive to future studies for evaluation of more subtle changes in fluorescence emission characteristics related to *in vitro* maturation such as formation of collagen crosslinks. Correlations of optical and ultrasonic parameters with results from traditional assays demonstrated the

potential of this bimodal technique as a noninvasive tool for monitoring tissue engineered cartilage.

Acknowledgments

This work was funded in part by the NIH Grant R01-HL67377 and R01-AR053286. The authors would also like to acknowledge Dr. K. Kirk Shung, Dr. Jonathan M. Cannata, and Hao-Chung Yang of the University of Southern California for providing the ultrasonic transducer used in the study. They would also like to thank Dr. Jennifer Phipps and Dr. Abhijit J. Chaudhari for their help in data and imaging processing, Dr. Grace Zhang, Dr. Yinghua Sun, and Matthew Lam for helping with the initial experiments.

Disclosure Statement

No competing financial interests exist.

References

1. Buckwalter, J.A., Saltzman, C., and Brown, T. The impact of osteoarthritis: implications for research. Clin Orthop Relat Res **427(Suppl),** S6, 2004.
2. Hu, J.C., and Athanasiou, K.A. A self-assembling process in articular cartilage tissue engineering. Tissue Eng **12,** 969, 2006.
3. Ofek, G., Revell, C.M., Hu, J.C., Allison, D.D., Grande-Allen, K.J., and Athanasiou, K.A. Matrix development in self-assembly of articular cartilage. PLoS One **3,** e2795, 2008.
4. Elder, B.D., and Athanasiou, K.A. Synergistic and additive effects of hydrostatic pressure and growth factors on tissue formation. PLoS One **3,** e2341, 2008.
5. Elder, B.D., and Athanasiou, K.A. Systematic assessment of growth factor treatment on biochemical and biomechanical properties of engineered articular cartilage constructs. Osteoarthritis Cartilage **17,** 114, 2009.
6. Natoli, R., Revell, C.M., and Athanasiou, KA. Chondroitinase ABC treatment results in increased tensile properties of self-assembled tissue engineered articular cartilage. Tissue Eng Part A **15,** 3119, 2009.
7. Natoli, R.M., Responte, D.J., Lu, B.Y., and Athanasiou, K.A. Effects of multiple chondroitinase ABC applications on tissue engineered articular cartilage. J Orthop Res [Epub ahead of print]; DOI: 10.1002/jor.20821. 2009.
8. Berezin, M.Y., and Achilefu, S. Fluorescence lifetime measurements and biological imaging. Chem Rev **110,** 2641, 2010.
9. Chorvat, D., and Chorvatova, A. Multi-wavelength fluorescence lifetime spectroscopy: a new approach to the study of endogenous fluorescence in living cells and tissues. Laser Phys Lett **6,** 175, 2009.
10. Svanberg, K., Klinteberg, C.a., Nilsson, A., Wang, I., Andersson-Engels, S., and Svanberg, S. Laser-based spectroscopic methods in tissue characterization. Ann N Y Acad Sci **838,** 123, 1998.
11. Kochiadakis, G.E., Chrysostomakis, S.I., Kalebubas, M.D., Filippidis, G.M., Zacharakis, I.G., Papazoglou, T.G., *et al.* The role of laser-induced fluorescence in myocardial tissue characterization: an experimental *in vitro* study. Chest **120,** 233, 2001.
12. Lakowicz, J.R. Principles of Fluorescence Spectroscopy. New York: Springer Science and Business Media, 2006.
13. Elson, D., Requejo-Isidro, J., Munro, I., Reavell, F., Siegel, J., Suhling, K., *et al.* Time-domain fluorescence lifetime imaging applied to biological tissue. Photochem Photobiol Sci **3,** 795, 2004.
14. Ashjian, P., Elbarbary, A., Zuk, P., DeUgarte, D.A., Benhaim, P., and Hedrick, M.H. Noninvasive *in situ* evaluation of osteogenic differentiation by time-resolved laser-induced fluorescence spectroscopy. Tissue Eng **10,** 411, 2004.
15. Fite, B.Z., Decaris, M., Sun, Y., Sun, Y., Lam, A., Ho, C.K., *et al.* Noninvasive multimodal evaluation of bioengineered cartilage constructs combining time-resolved fluorescence and ultrasound imaging. Tissue Eng Part C Methods **17,** 495, 2011.
16. Foster, F.S., Lockwood, G.R., Ryan, L.K., Harasiewicz, K.A., Berube, L., and Rauth, A.M. Principles and applications of ultrasound backscatter microscopy. IEEE Trans Ultrason Ferroelectr Freq Control **40,** 608, 1993.
17. McPherson, D.D. Tissue characterization by ultrasound: what is possible now? What will be possible? Echocardiography **8,** 77, 1991.
18. Kawasaki, M., Takatsu, H., Noda, T., Ito, Y., Kunishima, A., Arai, M., *et al.* Noninvasive quantitative tissue characterization and two-dimensional color-coded map of human atherosclerotic lesions using ultrasound integrated backscatter: comparison between histology and integrated backscatter images. J Am Coll Cardiol **38,** 486, 2001.
19. Langevin, H., Rizzo, D., Fox, J., Badger, G., Wu, J., Konofagou, E., *et al.* Dynamic morphometric characterization of local connective tissue network structure in humans using ultrasound. BMC Syst Biol **1,** 25, 2007.
20. Bridal, S.L., Fournier, C., Coron, A., Leguerney, I., and Laugier, P. Ultrasonic backscatter and attenuation (11–27 MHz) variation with collagen fiber distribution in *ex vivo* human dermis. Ultrason Imaging **28,** 23, 2006.
21. Wang, S.Z., Huang, Y.P., Saarakkala, S., and Zheng, Y.P. Quantitative assessment of articular cartilage with morphologic, acoustic and mechanical properties obtained using high-frequency ultrasound. Ultrasound Med Biol **36,** 512, 2010.
22. Sun, Y., Park, J., Stephens, D.N., Jo, J.A., Sun, L., Cannata, J.M., *et al.* Development of a dual-modal tissue diagnostic system combining time-resolved fluorescence spectroscopy and ultrasonic backscatter microscopy. Rev Sci Instrum **80,** 065104, 2009.
23. Sun, Y., Chaudhari, A.J., Lam, M., Xie, H., Yankelevich, D., Phipps, J., Liu, J., Fishbein, M.C., Cannata, J.M., Shung, K.K., and Marcu, L. Multimodal characterization of compositional, structural and functional features of atherosclerotic plaques. Biomed Opt Express **2,** 2288, 2011.
24. Almarza, A.J., and Athanasiou, K.A. Seeding techniques and scaffolding choice for tissue engineering of the temporomandibular joint disk. Tissue Eng **10,** 1787, 2004.
25. Athanasiou, K.A., Agarwal, A., and Dzida, F.J. Comparative study of the intrinsic mechanical properties of the human acetabular and femoral head cartilage. J Orthop Res **12,** 340, 1994.
26. Mow, V.C., Gibbs, M.C., Lai, W.M., Zhu, W.B., and Athanasiou, K.A. Biphasic indentation of articular cartilage—II. A numerical algorithm and an experimental study. J Biomech **22,** 853, 1989.
27. Lakowicz, J.R. Principles of Fluorescence Spectroscopy, 2nd edition. New York: Kluwer Academic/Plenum, 1999.
28. Zukauskas, A., Vitta, P., Kurilcik, N., Jursenas, S., and Bakiene, E. Characterization of biological materials by

frequency-domain fluorescence lifetime measurements using ultraviolet light-emitting diodes. Opt Mater **30,** 800, 2008.
29. Saarakkala, S., Wang, S.Z., Huang, Y.P., and Zheng, Y.P. Quantification of the optical surface reflection and surface roughness of articular cartilage using optical coherence tomography. Phys Med Biol **54,** 6837, 2009.
30. Forman, M.D., Malamet, R., and Kaplan, D. A survey of osteoarthritis of the knee in the elderly. J Rheumatol **10,** 282, 1983.
31. Armstrong, C., and Mow, V. Variations in the intrinsic mechanical properties of human articular cartilage with age, degeneration, and water content. J Bone Joint Surg Am **64,** 88, 1982.
32. Peterfy, C.G. Scratching the surface: articular cartilage disorders in the knee. Magn Reson Imaging Clin N Am **8,** 409, 2000.
33. Responte, D.J., Natoli, R.M., and Athanasiou, K.A. Collagens of articular cartilage: structure, function, and importance in tissue engineering. Crit Rev Biomed Eng **35,** 363, 2007.

Address correspondence to:
Laura Marcu, Ph.D.
Department of Biomedical Engineering
University of California Davis
451 Health Sciences Drive, GBSF 2513
Davis, CA 95616

E-mail: lmarcu@ucdavis.edu

Yang Sun, Ph.D.
Department of Biomedical Engineering
University of California Davis
451 Health Sciences Drive, GBSF 2513
Davis, CA 95616

E-mail: ywsun@ucdavis.edu

Received: June 20, 2011
Accepted: October 14, 2011
Online Publication Date: January 19, 2012